HHS Public Access

Author manuscript

Trends Biotechnol. Author manuscript; available in PMC 2017 September 15.

Published in final edited form as:

Trends Biotechnol. 2016 May ; 34(5): 420–433. doi:10.1016/j.tibtech.2016.02.001.

Photoacoustic molecular imaging: from multiscale biomedical applications towards early-stage theranostics

Yajing Liu[1], **Liming Nie**[1,*], and **Xiaoyuan Chen**[2,*]

[1]State Key Laboratory of Molecular Vaccinology and Molecular Diagnostics & Center for Molecular Imaging and Translational Medicine (CMITM), School of Public Health, Xiamen University, Xiamen 361102, China

[2]Laboratory of Molecular Imaging and Nanomedicine, National Institute of Biomedical Imaging and Bioengineering (NIBIB), National Institutes of Health (NIH), Bethesda, MD 20892, USA

Abstract

Photoacoustic imaging (PAI) has ushered in a new era of observing biotechnology and facilitated the exploration of fundamental biological mechanisms and clinical translational applications, which has attracted tremendous attention in recent years. By converting laser into ultrasound emission, PAI combines rich optical contrast, high ultrasonic spatial resolution, and deep penetration depth in a single modality. This evolutional technique enables multiscale and multicontrast visualization from cells to organs, anatomy to function, and molecules to metabolism with high sensitivity and specificity. The state-of-the-art developments and applications of PAI are described in this review. Future prospects to clinical use are also highlighted. Collectively, PAI holds great promise to drive biomedical applications towards early-stage theranostics.

Keywords

Photoacoustic imaging; multiscale biomedical application; early stage theranostics; smart contrast agents

1. Principles and significance of PAI

Photoacoustic (PA) imaging (PAI), by converting incident photons into ultrasound waves, ultrasonically overcomes the optical diffusion limit (Figure 1) [1, 2]. Thus, PAI combines the rich contrast of optical imaging with the high resolution and deep penetration of ultrasound imaging. With the rapid development of laser technology and ultrasound detection, PAI has enabled scalable visualization at levels from organelles to organs and has attracted tremendous attention in the past few years [3]. This new emerging, noninvasive, and

*Correspondence to nielm@xmu.edu.cn (L Nie); shawn.chen@nih.gov (X Chen).

nonionizing imaging technique can unveil different physiopathological processes and disease states in a wide range of biomedical applications [4].

By integrating fine optical focusing and advanced scanning techniques, PA microscopy (PAM) is capable of single organelle and cell imaging in real-time [5]. PAM is sensitive enough to capture subtle changes of disease microenvironments, including nutrition supply capillaries, drug pharmacokinetics, and local acidity [6, 7]. Specifically, PAM can track functional cellular or subcellular activities such as cell entanglement after labeling with different dyes at unprecedented depth, which cannot be achieved by photo-activated localization microscopy (PALM), stochastic optical reconstruction microscopy (STORM), two-photon microscopy, or confocal microscopy. PA endoscopy (PAE) can provide structural and functional information of the esophagus and gastrointestinal tract [8]. In addition to direct images of internal structure, PA images have also been measured from tissue surfaces by a hand-held PA array transducer [9]. At the macroscopic level, PA computed tomography (PACT) allows brain, organ, and whole body imaging from small animals to primates [10].

Recently, PAI has received immense attention as a promising means for diagnostic and therapeutic monitoring purposes. In this review, we will elucidate the recent advances in PAI in detail, followed by its potential applications for early-stage theranostics. The future development trends, clinical outlook, and potential limitations are also discussed. We hope this review will open up new visions to inspire a wider range of scientific discoveries for fundamental life science and clinical translation.

2. Specific embodiments of PAI

2.1 Microscopic level PAM

PAM, which possesses ultrahigh sensitivity to light absorption, is a powerful technique that plays a unique role in imaging biological samples at multiple spatiotemporal scales. In this section, we examine the advanced techniques and the state-of-the-art instrumental embodiments of PAM in biomedicine, and we summarize their enormous potentials towards clinical applications.

2.1.1 Main-stream PAM—By employing raster scanning of its acoustic or optical focus, PAM can form 3D images directly from acquired PA signals. Based on different focusing types, PAM can be implemented as either optical-resolution PAM (OR-PAM) or acoustic-resolution PAM (AR-PAM). In OR-PAM, the optical focus is tighter than the acoustic focus, which provides the system optically defined lateral resolution. Due to high spatial resolution, OR-PAM has promoted technology advances to millisecond timescales and submicron length scales (Figure 2A). In AR-PAM, the acoustic focus is smaller than optical focus. As the acoustically defined lateral resolution is not affected by optical scattering, AR-PAM refers to a focused acoustic transducer that collects PA signals for imaging targets at depths beyond the diffusive limit (Figure 2B). In particular, the combination of newly developed functional contrast agents and advanced engineering mechanisms has pushed PAM to further uncover subtle changes of disease microenvironments. Additionally, these advances have allowed PAM to monitor single organelles and cells such as melanosomes, mitochondria, circulating tumor cells (CTCs), and red blood cells (RBCs) in real-time. Jim *et al.* introduced

a fast and cost-effective OR-PAM system that exploited a 2-axis microelectromechanical system (MEMS) scanner to achieve a wide scanning region and high spatial resolution (Figure 2A). A PA image from a mouse ear showed that not only small capillaries but also individual RBCs were clearly captured [11].

However, in strongly scattering biological tissue, incident light is greatly attenuated by the photon heterogeneous wavelength-scale refractive index, which greatly confines the application range of PAM [12]. To overcome the scattering limitation in biological tissue, a variety of advanced wavefront shaping technologies have been recently proposed and developed [13, 14]. Judkewitz *et al.* proposed a time reversal of variance encoded light (TROVE) method to fundamentally overcome the resolution limit [15]. In the TROVE focusing method, multiple randomized input photons were encoded and decoded by a unique variance structure to unmix individual optical modes (Figure 2C). Thus these modes were time reversed, and speckle-sized optical focusing could be achieved. Depending on the time reversal of the variance encoded wavefront, a lateral resolution of ~5 μm was achieved.

For biomedical applications, PA-based wavefront engineering is superior to the light focus of optical microscopy and can non-invasively focus light deeply into the scattering media [16, 17]. In order to improve both the signal-to-noise ratio (SNR) and the resolution, Conkey *et al.* combined the Gaussian-shape spatial sensitivity of a focused ultrasonic transducer to a PA wave with different competitive modes (Figure 2D) [18]. The experimental results illustrated that the SNR and spatial resolution in PAI from a scattering target were improved by factors of approximately 10 and 5, respectively. Another method, developed by Lai *et al.*, produced nonlinear PA signals based on the Grueneisen relaxation effect to guide iterative wavefront optimization [19].

With high laser repetition, rapid imaging speed, and wavefront optimization engineering, PAM is able to map vascular morphology, oxygen saturation, oxygen metabolism, and blood flow. This technology has widespread applications for functional imaging and early-stage diagnosis of diseases.

2.1.2 New adaptations of PAM—The integration of PAM and flow cytometry (PAFC) can yield a valuable research tool in animal models of human diseases to provide ultrasensitive detection of pathogens, CTCs, pharmacokinetics of drugs, contrast dyes, and nanoparticles *in vivo*. In contrast to conventional flow cytometry, a PAFC setup is composed of three main parts: a pulsed laser, a microscopic imaging system, and an ultrasound transducer (Figure 3A) [20]. Based on the PA effect instead of fluorescence detection, PAFC has a high threshold sensitivity *in vivo* for noninvasive real-time imaging [21].

To capture CTCs, a fundamental challenge for existing assays is the low concentration of 1–10 CTC/mL blood in a 5–10 mL volume. Due to advanced developments of high repetition-rate lasers [22], PAFC has been exploited as a promising candidate to overcome the shortcomings with functional PA agents. Nedosekin *et al.* used magnetic enriched nanoparticles to increase PA signals of CTCs and suppress background signals from intrinsic optical absorbers at the same time [23]. By combination of CTC photothermal therapy and nanobubble-enhanced diagnosis, Galanzha *et al.* suggested that PAFC can be exploited as an

excellent clinical tool for well-timed theranostics [24]. A portable device and a wavelength tunable diode laser will likely further push PAFC to translational applications.

Oxygen metabolism is an essential physiological process that provides nutrients to maintain regular life activity [25]. As delivery vehicles, RBCs are the fundamental elements for transporting oxygen to aerobic cells and tissues. The real-time label-free imaging of oxygen delivery *via* flowing RBCs has far-reaching significance for oxygenation-related diseases such as mental disorders and tumor angiogenesis. Coupling micrometer-scale spatial resolution with millisecond-scale temporal resolution, PA flowoxigraphy (PA FOG), a promising frontier of OR-PAM, offers a comprehensive illustration of oxygen functional parameters *in vivo* (Figure 3B) [26, 27]. The benefits of PA FOG include high detection sensitivity by label-free RBC imaging and dual wavelength spectrophotometry measurement in reflection mode. With a 20-Hz B-scan video speed and 20-μs dual-wavelength switching time, PA FOG was fast enough to detect oxygenation in single RBCs flowing and unveiled the strong relationship of multifunctional oxygen metabolic parameters at the single-cell level in the brain. PA FOG uncovered the strong relationship of multifunctional oxygen metabolic parameters at single-cell level in the brain.

Förster resonance energy transfer (FRET) mechanism has recently been introduced in PA as a valuable tool to improve imaging depth [28, 29]. FRET microscopy refers to the nonradiative transfer of excited photons from a donor to an accepter to emit fluorescence [30]. However, light diffusion prevents FRET microscopy to image depth beyond optical mean free path (~1 mm). Integrating the FRET mechanism with PAM (FRET-PAM) where donor FRET energy is absorbed to generate acoustic waves through accepter thermal expansion, produces significantly enhanced PA signals (Figure 3C). To illustrate this principle, Wang *et al.* employed a fluorescent donor R6G and a nonfluorescent acceptor DQOCI as a FRET pair [29]. Compared with fluorescence microscopy, FRET-PAM efficiently increased the penetration depth to image samples 1 cm under mouse skin tissue.

Recent developments of PA and traditional endoscopy techniques have been introduced in internal organs including the gastrointestinal (GI) tract, the esophagus, the colon, and atherosclerotic plaques [31]. PA endoscopy (PAE) has the potential for the precise localization of lesions, early detection of neoplasm metastasis, and noninvasive visualization of submucosal diseases *in situ* [8, 32].

A myriad of biomedical PAE implements, conceptually similar to conventional ultrasound endoscopy, have been exploited for preclinical applications. The unique properties of interior wall detection and visible structural information facilitate ultrasound (US) a consequential add-on to PAE [33, 34]. By using a scanning mirror system rather than traditional mechanical scanning, PAE probe allows circumferential scanning, and both laser beams and ultrasonic waves can be reflected to the targeted sites without moving the ultrasonic detector. Then, both PA and US signals are sequentially received by the same ultrasonic transducer (Figure 3D) [35]. By taking advantage of this well-equipped PAE system, Yang *et al.* acquired *in vivo* 3D images of the vasculature distribution in rabbit esophagi.

In contrast to one-mode PAE, the co-registered PAE/US system displayed both functional and physiological information. For example, Evans blue gathering in the lymph node was observed, and the vasculature and adjacent colon were characterized [36]. For PAE, however, probe size and motion artifacts are major issues in clinical practice, which could be mitigated by miniaturized elements and sophisticated image reconstruction [35].

2.2 Macroscopic level PACT

PACT systems usually utilize a bright-field laser beam to illuminate a relatively large region-of-interest (ROI). PA signals are detected by unfocused or focused ultrasonic transducers. Then, high-resolution images can be reconstructed on the basis of an inverse algorithm such as back projection or time-reversed algorithms [37, 38]. Commonly configured ultrasound transducers fall into three categories: circular, spherical, and planar geometries. These transducers have been implemented in both small animal imaging and human imaging.

2.2.1 Circular detection system—A circular detection system can be created by positioning 10 fiber bundles to create a cylindrical ring illumination and arranging a 64-element detector array over a curved surface for parallel-data acquisition, as described by Razansky *et al*. [39]. By video-rate imaging of tissue at multiple wavelengths and subsequent spectral unmixing algorithms, the multispectral optoacoustic tomography (MSOT) system has achieved significant advances for translating PA to bedside applications, such as breast neuroimaging, cardiovascular disease, and vascular imaging [40–44]. Figure 4A clearly showcases the capability of the MSOT system to recognize deep structural features in mice [45]. However, the top portion of the structure along the elevational axis was not clearly illustrated due to incomplete detection views [46].

More work should be done to circumvent this type of detector’s bottlenecks, some of which include inhomogeneous spatial resolution, limited imaging depth, and acoustic mismatches especially for the human skull [39, 47]. PACT with a high frame rate, tunable laser sources, a well-designed acoustic array and a corresponding reconstruction algorithm are necessary to attract more clinical attention. PACT combined with other imaging modalities, especially with ultrasound (US), positron emission tomography (PET) and optical coherence tomography (OCT), will add complementary information and provide new insights in biomedicine.

2.2.2 Spherical detection system—As PA signals propagate in every possible direction relative to the detector, detecting pressures from all solid angles is of great significance. A variant PACT scanning system that exploits spherical scanning has notable merits to achieve a homogenous and isotropic special resolution [46].

The hemispherical PA imaging system is a newly emerging, powerful, and non-invasive imaging mode *in vivo*. 128 flat transducers, which can collect PA signals simultaneously, are spirally located on the surface of a bowl (Figure 4B) [48]. The 128-chaneled parallel data-acquisition system can acquire a volumetric image in as little as 6 s. Owing to the special bowl configuration, the hemispherical instrument can receive PA signals from as many solid angles as possible, resulting in an isotropic spatial resolution of 250 μm over a 2.5 × 2.5 × 2.5 cm^3 field of view (FOV). A near infrared (NIR) wavelength-tunable laser as the

excitation source can penetrate deeply in biological tissue, which may reach as deep as 4 cm in human breast [49, 50]. Meanwhile, the optical intensity of the laser is 1 to 2 orders of magnitude lower than the maximum permissible exposure (MPE), which guarantees its safety in living subjects.

2.2.3 Planar detection system—Planar array-based PACT can be implemented by taking advantage of commercial 2-D matrices [51] or phased [52] or linear acoustic transducer arrays [53]. Because of their inexpensive cost, hand-held probes, and co-registered PA/US imaging characterization, linear scanner arrays have been widely applied for PACT with much more clinical availability than circular or spherical detectors. As displayed in Figure 4C, exploiting a laser with 20 Hz repetition rate and a 256-element linear transducer array with 40 MHz center frequency, a full-view PACT system was capable of acquiring an accurate image of a zebrafish *in vivo*. Since image mismatches and artifacts exist, a multiview Hilbert transformation approach was proposed to generate a 60 μm spatial resolution within a 10×10 mm^2 FOV [54].

In another report, a 256-element PA linear array along with an ultrasonic thermal encoding transducer was developed for mouse vascular volumetric imaging *in vivo* [55]. The PA wave amplitude from the encoded spots was increased, so the imaging of full-view vessels was remarkably enhanced. However, the PA image quality from these instruments is still suboptimal because of a low center frequency, a finite aperture, a low sensitivity, and a slow imaging speed. Further advances, such as dedicated reconstruction algorithms, high laser repetition rates, and high-speed data read-out times, are imperative to promote PACT systems for clinical accessibility.

3. Disease detection by PAI with various contrasts

3.1 Multi-parameter PAI with versatile contrasts

The cause of disease is a multistep and complicated process that can induce changes in the tissue microenvironment, such as angiogenesis in breast tissue, melanin deposition in skin cancers, lipid accumulation in atherosclerosis, and pH fluctuation in cancer metastasis. Endogenous chromophores including oxyhemoglobin (HbO_2) [56], deoxyhemoglobin (Hb) [57], fat [58], melanin [59], nucleic acids [60], and water [61] possess various characteristics of absorption spectra (Figures 5A–5C). PAT, based on the specific spectrum of a given chromophore, can be applied to monitor and quantify the hallmarks of cancers. A combination of intrinsic and dynamic oxyhemoglobin and deoxygenated hemoglobin from blood vessel enables multi-parameter PAT to comprehensively reflect physiological and pathological information including blood perfusion, the oxygen saturation (sO_2), and the metabolic rate of oxygen (MO_2) [7]. Based on the Doppler effect, PA flowmetry can also measure blood flow in a living mouse with high sensitivity [62]. Consequently, along with parameters from endogenous agents, metabolic PAT may play a valuable role in accelerating early cancer screening *in vivo*.

With the rapid development of imaging technologies and different implementation of PA, there is a fast-growing category of exogenous contrast agents designed for tracking or visualizing biological processes, especially in sentinel lymph node (SLN) mapping, glioma

and breast cancer detection, and other applications. [63–65]. According to their principle, material and function, these fabricated PA contrast agents can be divided into five classes: gene products [66], organic dyes [67], fabricated nanoparticles [63, 68], multimodality agents, and theranostic agents [69].

Gene products have attracted great attention for PA applications on the basis of their specific genetic expression, strong absorption, and selective labeling of cells. Beard *et al.* showed that a tyrosinase-based reporter is a powerful tool for deep PA in mammalian tissues at depths approaching 10 mm (Figure 5D) [66]. The fluorescent protein iRFP which is specifically engineered by bacterial phytochrome, holds great potential to provide high tissue-specific PA contrast to unveil tumor growth processes and track metastases in deep tissue [70].

Analogous to gene products, organic dyes such as methylene blue (MB), indocyanine-green (ICG), Evans blue (EB), IRDye800CW, and MMPSense™ 680, can also be used as candidates for functional PA imaging. Methylene blue (MB), for instance, is an FDA approved agent that can be employed for multimodal SLN detection [71]. A noninvasive PA method was used to visualize nanoformulated naphthalocyanine intestinal accumulation and enabled intestinal imaging with co-registered ultrasound (Figure 5E) [67].

Due to strong surface plasmon resonance (SPR), tunable optical absorption, and effective optical-to-acoustic conversion, metal nanoparticles, like gold nanoparticles and silver nanoparticles, have attracted extensive attention for PA applications. For example, versatile shapes and sizes of gold nanoparticles, such as nanorods, nanospheres, nanocages, nanoshells, nanoclusters, nanobeacons, and nanostars, can be tuned to exhibit absorption peaks in the NIR region for personalized biomedical applications. Song *et al.* showed that systemically administered poly(ethylene glycol) (PEG) -poly(lactic-co-glycolic acid) (PLGA) coated gold nanoparticles can be used as an ultrasmall contrast agent (~60 nm) for efficient tumor therapy, and these particles can be tracked by PAT [72]. Besides plasmonic nanoparticles, there are other types of nanoparticles such as carbon nanoparticles [6], quantum dots (QD) [73], iron oxide [74], semiconducting polymer nanoparticles [75, 76], and others.

Coupled with ideal contrast agents, PA molecular imaging can provide remarkable anatomic and functional information. Tumor margin evaluation is essential to increase tumor contrast and is desirable to improve prognoses (Figure 5E) [77]. In this respect, a trimodality nanocomposite that integrated MRI-PA-Raman imaging was designed to achieve accurate brain tumor localization and resection (Figure 5G) [63].

3.2 PAI for early-stage theranostics

Ideally with appropriate intrinsic physicochemical properties or appropriate labels, nanomaterials have emerged as potential building templates that synergistically hybridize the modalities of diagnosis and therapy. These theranostic nanoparticles would allow us to diagnose disease (Figures 6A–6D) [78–80], track the kinetics of the particles (Figure 6E) [81], and evaluate treatment efficacy (Figure 6F) [6] by PAT or uniting multimodal platforms [82]. Bai *et al.* improved the capability of magnetic-hollow gold nanospheres to provide a

stable T2-weighted MRI contrast and enhanced PA signal, which manifested excellent imaging ability of cancer cells. These gold nanospheres thus made this nanocomposite a potential theranostic nanoagent for effective diagnosis and MRI-PAT-guided photothermal therapy (PTT) [69]. Not only for disease diagnosis, PA with the synergistic effects of functional molecular probes has become a new trend to propel the biomedical field toward early-stage theranostics and personalized medicine [83]. In one study, doxorubicin-graphene oxide-based nanoparticles were well engineered and noninvasively monitored by a sensitive PAM. The results clearly indicated inhibition of tumor angiogenesis within 4 days after therapy [6].

In recent years, the use of effective theranostic agents has become an attractive trend to apply PAT for early diagnosis, precise localization, tumor staging, curative effect assessment, and image-guided surgery. However, for further biomedical applications, rigorous principles should be followed when using contrast agents in humans; for instance, biosafety, availability, compatibility, and cost effectiveness must all be considered.

4. Summary and clinical outlook

Early diagnosis is an important factor for improving clinical outcomes. During surgery, sensitive and specific imaging tools suited for accurately mapping and determining the status of tumor are sought after to circumvent the drawbacks of traditional imaging methods, such as the side effects of radiation, high cost, long time consuming, and variability between different operators. In this regard, noninvasive PA imaging, with tailored and well-selected contrast agents, can visualize and quantitatively evaluate small lesions. The unique optical and ultrasonic characteristics of PA, such as real-time imaging and volumetric imaging capacity, and compatibility with clinical imaging tools, have elicited increasing research interest in recent years.

With several commercial PA systems and new implementations, a trend has emerged to use PAT as a diagnostic tool in cancer and cardiovascular diseases (Table 1). For example, a brain cortex was successfully imaged through an intact adult human skull with a PAT system, in which a photo recycler and a subtraction method were employed to improve the PA SNR [10]. Heijblom *et al.* modified the Twente PA Mammoscope for breast imaging. They acquired a high PA contrast in malignancies and investigated the clinical feasibility of PAT in patient studies [84]. Another major application of translational PAT is SLN mapping. With a FDA approved agent, methylene blue, SLN mapping has been detected clinically by a hand-held PA probe [64].

From structure to function, from table-top to hand-held, from diagnosis to theranostic, there is an overwhelming trend for using PAT in bedside clinics. Certain diseases can be diagnosed at an early stage before they have the chance to metastasize or deteriorate and are therefore more likely to be cured. While exciting breakthroughs have been made, PAT still suffers from certain technical hurdles, such as large probe size, motion artifacts, inaccurate algorithms, and slow imaging speed (see the Outstanding Questions Box). To accelerate the translation of PAI from the bench to the bedside, user-friendly hardware is desirable to

enhance its robustness and performance; fast, accurate, and easy-to-follow read-outs are necessary for physicians to make precise diagnoses.

On the other hand, more FDA (Food and Drug Administration) approved compounds are needed to promote PAI for human use. However, it would take a long time to undergo a rigorous government approval process. Multidisciplinary professionals including scientists, clinicians, biologist, chemists, and government employees should collaborate to advance the technique for early-stage theranostics. Overcoming the aforementioned limitations will definitely strengthen the position of PAT in biomedical practice. Integrating with further technical progress will advance the translation of PAI towards early-stage theranostics in the clinic.

Acknowledgments

This work was supported by National Basic Research Program of China (863 Program 2015AA020502), the National Science Foundation of China (81571744, 81301257), and the Intramural Research Program (IRP), National Institute of Biomedical Imaging and Bioengineering (NIBIB), National Institutes of Health (NIH).

References

1. Wang L, et al. Ultrasonically encoded photoacoustic flowgraphy in biological tissue. Phys. Rev. Lett. 2013; 111:204301. [PubMed: 24289689]
2. Zharov VP. Ultrasharp nonlinear photothermal and photoacoustic resonances and holes beyond the spectral limit. Nat. Photonics. 2011; 5:110–116. [PubMed: 25558274]
3. Wang LV, Hu S. Photoacoustic tomography: in vivo imaging from organelles to organs. Science. 2012; 335:1458–1462. [PubMed: 22442475]
4. Mallidi S, et al. Photoacoustic imaging in cancer detection, diagnosis, and treatment guidance. Trends Biotechnol. 2011; 29:213–221. [PubMed: 21324541]
5. Hu S, Wang LV. Optical-resolution photoacoustic microscopy: auscultation of biological systems at the cellular level. Biophys. J. 2013; 105:841–847. [PubMed: 23972836]
6. Nie L, et al. Early-stage imaging of nanocarrier-enhanced chemotherapy response in living subjects by scalable photoacoustic microscopy. ACS Nano. 2014; 8:12141–12150. [PubMed: 25406986]
7. Yao J, et al. High-speed label-free functional photoacoustic microscopy of mouse brain in action. Nat. Methods. 2015; 12:407–410. [PubMed: 25822799]
8. Yang JM, et al. Optical-resolution photoacoustic endomicroscopy in vivo. Biomed. Exp. 2015; 6:918–932.
9. Zhou Y, et al. Handheld photoacoustic microscopy to detect melanoma depth in vivo. Opt. Lett. 2014; 39:4731–4734. [PubMed: 25121860]
10. Nie L, et al. Photoacoustic tomography through a whole adult human skull with a photon recycler. J. Biomed. Opt. 2012; 17:110506. [PubMed: 23123972]
11. Kim JY, et al. Fast optical-resolution photoacoustic microscopy using a 2-axis water-proofing MEMS scanner. Sci. Rep. 2015; 5:7932. [PubMed: 25604654]
12. Yao J, et al. Multiscale Functional and Molecular Photoacoustic Tomography. Ultrasonic Imaging. 2016; 38:44–62. [PubMed: 25933617]
13. Lv XX, et al. Time-reversed ultrasonically encoded optical focusing into scattering media. Nat. Photonics. 2011; 5:154–157. [PubMed: 21532925]
14. Tay JW, et al. Ultrasonically encoded wavefront shaping for focusing into random media. Sci. Rep. 2014; 4:3918. [PubMed: 24472822]
15. Judkewitz B, et al. Speckle-scale focusing in the diffusive regime with time-reversal of variance-encoded light (TROVE). Nat. Photonics. 2013; 7:300–305. [PubMed: 23814605]
16. Chaigne T, et al. Improving photoacoustic-guided optical focusing in scattering media by spectrally filtered detection. Opt. Lett. 2014; 39:6054–6057. [PubMed: 25361154]

17. Chaigne T, et al. Controlling light in scattering media non-invasively using the photoacoustic transmission matrix. Nat. Photonics. 2014; 8:59–65.
18. Conkey DB, et al. Super-resolution photoacoustic imaging through a scattering wall. Nat. Comm. 2015; 6:7902.
19. Lai P, et al. Photoacoustically guided wavefront shaping for enhanced optical focusing in scattering media. Nat. Photonics. 2015; 9:126–132. [PubMed: 25914725]
20. Galanzha EI, Zharov VP. Photoacoustic flow cytometry. Methods. 2012; 57:280–296. [PubMed: 22749928]
21. Wang LV, Gao L. Photoacoustic microscopy and computed tomography: from bench to bedside. Ann. Rev. Biomed. Eng. 2014; 16:155–185. [PubMed: 24905877]
22. DA N, et al. Ultra-fast photoacoustic flow cytometry with a 0.5 MHz pulse repetition rate nanosecond laser. Opt. Express. 2010; 18:8605. [PubMed: 20588705]
23. Nedosekin DA, et al. In Vivo Ultra-Fast Photoacoustic Flow Cytometry of Circulating Human Melanoma Cells Using Near-Infrared High-Pulse Rate Lasers. Cytometry Part A. 2011; 79A:825–833.
24. Galanzha EI, Zharov VP. Circulating Tumor Cell Detection and Capture by Photoacoustic Flow Cytometry in Vivo and ex Vivo. Cancers (Basel). 2013; 5:1691–1738. [PubMed: 24335964]
25. Yao J, et al. Label-free oxygen-metabolic photoacoustic microscopy in vivo. J. Biomed. Opt. 2011; 16:076003. [PubMed: 21806264]
26. Lidai W, et al. Single-cell label-free photoacoustic flowoxigraphy in vivo. Proc. Nat. Acad. Sci. U. S. A. 2013; 110:5759–5764.
27. Wang L, et al. Fast voice-coil scanning optical-resolution photoacoustic microscopy. Opt. Lett. 2011; 36:139–141. [PubMed: 21263479]
28. Qin H, et al. Fluorescence Quenching Nanoprobes Dedicated to In Vivo Photoacoustic Imaging and High-Efficient Tumor Therapy in Deep-Seated Tissue. Small. 2015; 11:2675–2686. [PubMed: 25656695]
29. Wang Y, Wang LV. Forster resonance energy transfer photoacoustic microscopy. J. Biomed. Opt. 2012; 17:086007. [PubMed: 23224194]
30. Yamashita H, et al. Oligomerization-function relationship of EGFR on living cells detected by the coiled-coil labeling and FRET microscopy. Biochim. Biophys. Acta. 2015; 1848:1359–1366. [PubMed: 25771448]
31. Meng J, Song L. Biomedical photoacoustics in China. Photoacoustics. 2013; 1:43–48. [PubMed: 25300898]
32. Zackrisson S, et al. Light in and sound out: emerging translational strategies for photoacoustic imaging. Cancer Res. 2014; 74:979–1004. [PubMed: 24514041]
33. Yoon TJ, Cho YS. Recent advances in photoacoustic endoscopy. World journal of gastrointestinal endoscopy. 2013; 5:534–539. [PubMed: 24255745]
34. Kim J, et al. Photoacoustic imaging platforms for multimodal imaging. Ultrasonography (Seoul, Korea). 2015; 34:88–97.
35. Yang JM, et al. Three-dimensional photoacoustic endoscopic imaging of the rabbit esophagus. PloS One. 2015; 10:e0120269. [PubMed: 25874640]
36. Yang JM, et al. Simultaneous functional photoacoustic and ultrasonic endoscopy of internal organs in vivo. Nat. Med. 2012; 18:1297–1302. [PubMed: 22797808]
37. Huang C, et al. Aberration correction for transcranial photoacoustic tomography of primates employing adjunct image data. J. Biomed. Opt. 2012; 17:066016. [PubMed: 22734772]
38. Huang C, et al. Photoacoustic computed tomography correcting for heterogeneity and attenuation. J. Biomed. Opt. 2012; 17:061211. [PubMed: 22734741]
39. Razansky D, et al. Volumetric real-time multispectral optoacoustic tomography of biomarkers. Nat. Protoc. 2011; 6:1121–1129. [PubMed: 21738125]
40. E, dB, et al. Optical innovations in surgery. Br. J. Surg. 2015; 102:e56–e72. [PubMed: 25627136]
41. Taruttis A, et al. Multispectral optoacoustic tomography of myocardial infarction. Photoacoustics. 2013; 1:3–8. [PubMed: 25327410]

42. Burton NC, et al. Multispectral opto-acoustic tomography (MSOT) of the brain and glioblastoma characterization. NeuroImage. 2013; 65:522–528. [PubMed: 23026761]
43. Yao J, et al. Noninvasive photoacoustic computed tomography of mouse brain metabolism in vivo. SPIE BiOS. 2013:257–266.
44. Taruttis A, et al. Mesoscopic and macroscopic optoacoustic imaging of cancer. Cancer Res. 2015; 75:1548–1559. [PubMed: 25836718]
45. Taruttis A, Ntziachristos V. Advances in real-time multispectral optoacoustic imaging and its applications. Nat. Photonics. 2015; 9:219–227.
46. Xia J, Wang LV. Small-animal whole-body photoacoustic tomography: a review. IEEE Trans. Biomed. Eng. 2014; 61:1380–1389. [PubMed: 24108456]
47. Cremet L, et al. Pathogenic potential of Escherichia coli clinical strains from orthopedic implant infections towards human osteoblastic cells. Pathogens and disease. 2015; 73:ftv065. [PubMed: 26333570]
48. Nie L, et al. In vivo volumetric photoacoustic molecular angiography and therapeutic monitoring with targeted plasmonic nanostars. Small. 2014; 10:1585–1593. 1441. [PubMed: 24150920]
49. Xia J, et al. Photoacoustic tomography: principles and advances. Electromagnetic waves (Cambridge, Mass.). 2014; 147:1–22.
50. Kruger RA, et al. Photoacoustic angiography of the breast. Med. Phys. 2010; 37:6096–6100. [PubMed: 21158321]
51. Wang Y, et al. In vivo three-dimensional photoacoustic imaging based on a clinical matrix array ultrasound probe. J. Biomed. Opt. 2012; 17:061208. [PubMed: 22734738]
52. Erpelding TN, et al. Sentinel lymph nodes in the rat: noninvasive photoacoustic and US imaging with a clinical US system. Radiology. 2010; 256:102–110. [PubMed: 20574088]
53. Gateau J, et al. Three-dimensional optoacoustic tomography using a conventional ultrasound linear detector array: whole-body tomographic system for small animals. Med. Phys. 2013; 40:013302. [PubMed: 23298121]
54. Li G, et al. Multiview Hilbert transformation for full-view photoacoustic computed tomography using a linear array. J. Biomed. Opt. 2015; 20:066010. [PubMed: 26112369]
55. Wang L, et al. Ultrasonic-heating-encoded photoacoustic tomography with virtually augmented detection view. Optica. 2015; 2:307–312. [PubMed: 25984555]
56. Bohndiek SE, et al. Photoacoustic Tomography Detects Early Vessel Regression and Normalization During Ovarian Tumor Response to the Antiangiogenic Therapy Trebananib. J. Nucl. Med. 2015; 56:1942–1947. [PubMed: 26315834]
57. Luke GP, Emelianov SY. Optimization of in vivo spectroscopic photoacoustic imaging by smart optical wavelength selection. Opt. Lett. 2014; 39:2214–2217. [PubMed: 24686714]
58. Guggenheim JA, et al. Photoacoustic imaging of human lymph nodes with endogenous lipid and hemoglobin contrast. J. Biomed. Opt. 2015; 20:50504. [PubMed: 26008874]
59. Strohm EM, et al. High frequency label-free photoacoustic microscopy of single cells. Photoacoustics. 2013; 1:49–53. [PubMed: 25302149]
60. Cao R, et al. Multispectral photoacoustic microscopy based on an optical-acoustic objective. Photoacoustics. 2015; 3:55–59. [PubMed: 26236641]
61. Xu Z, et al. Photoacoustic tomography of water in phantoms and tissue. J. Biomed. Opt. 2010; 15:036019. [PubMed: 20615021]
62. Brunker J, Beard P. Pulsed photoacoustic Doppler flowmetry using time-domain cross-correlation: accuracy, resolution and scalability. J. Acoust. Soc. Am. 2012; 132:1780–1791. [PubMed: 22978905]
63. Kircher MF, et al. A brain tumor molecular imaging strategy using a new triple-modality MRI-photoacoustic-Raman nanoparticle. Nat. Med. 2012; 18:829–834. [PubMed: 22504484]
64. Kim C, et al. Performance benchmarks of an array-based hand-held photoacoustic probe adapted from a clinical ultrasound system for non-invasive sentinel lymph node imaging. Philos. Trans. A Math Phys. Eng. Sci. 2011; 369:4644–4650. [PubMed: 22006911]
65. Chen D, et al. Theranostic applications of carbon nanomaterials in cancer: Focus on imaging and cargo delivery. J. Control. Release. 2015; 210:230–245. [PubMed: 25910580]

66. Jathoul AP, et al. Deep in vivo photoacoustic imaging of mammalian tissues using a tyrosinase-based genetic reporter. Nat. Photonics. 2015; 9:239–246.
67. Zhang Y, et al. Non-invasive multimodal functional imaging of the intestine with frozen micellar naphthalocyanines. Nat. Nanotechnol. 2014; 9:631–638. [PubMed: 24997526]
68. Tang Y, et al. An aptamer-targeting photoresponsive drug delivery system using "off-on" graphene oxide wrapped mesoporous silica nanoparticles. Nanoscale. 2015; 7:6304–6310. [PubMed: 25782595]
69. Bai LY, et al. Multifunctional magnetic-hollow gold nanospheres for bimodal cancer cell imaging and photothermal therapy. Nanotechnology. 2015; 26:315701. [PubMed: 26177713]
70. Krumholz A, et al. Multicontrast photoacoustic in vivo imaging using near-infrared fluorescent proteins. Sci. Rep. 2014; 4:3939. [PubMed: 24487319]
71. Akers WJ, et al. Multimodal sentinel lymph node mapping with single-photon emission computed tomography (SPECT)/computed tomography (CT) and photoacoustic tomography. Transl. Res. 2012; 159:175–181. [PubMed: 22340767]
72. Song J, et al. Ultrasmall Gold Nanorod Vesicles with Enhanced Tumor Accumulation and Fast Excretion from the Body for Cancer Therapy. Adv. Mater. 2015; 27:4910–4917. [PubMed: 26198622]
73. Hembury M, Chiappini C. Gold-silica quantum rattles for multimodal imaging and therapy. 2015; 112:1959–1964.
74. Chen PJ, et al. Multitheragnostic Multi-GNRs Crystal-Seeded Magnetic Nanoseaurchin for Enhanced In Vivo Mesenchymal-Stem-Cell Homing, Multimodal Imaging, and Stroke Therapy. Adv. Mater. 2015; doi: 10.1002/adma.201502784
75. Pu K, et al. Diketopyrrolopyrrole-Based Semiconducting Polymer Nanoparticles for In Vivo Photoacoustic Imaging. Adv. Mater. 2015; 27:5184–5190. [PubMed: 26247171]
76. Pu K, et al. Semiconducting polymer nanoparticles as photoacoustic molecular imaging probes in living mice. Nat. Nanotechnol. 2014; 9:233–239. [PubMed: 24463363]
77. Nie L, et al. Palladium nanosheets as highly stable and effective contrast agents for in vivo photoacoustic molecular imaging. Nanoscale. 2014; 6:1271–1276. [PubMed: 24317132]
78. Menke J. Photoacoustic breast tomography prototypes with reported human applications. Eur. Radiol. 2015; 25:2205–2213. [PubMed: 25721319]
79. Luke GP, et al. Silica-coated gold nanoplates as stable photoacoustic contrast agents for sentinel lymph node imaging. Nanotechnology. 2013; 24:455101. [PubMed: 24121616]
80. Rajian JR, et al. Photoacoustic tomography to identify inflammatory arthritis. J. Biomed. Opt. 2012; 17:96013–96011. [PubMed: 23085914]
81. Li W, et al. In vivo quantitative photoacoustic microscopy of gold nanostar kinetics in mouse organs. Biomed. Exp. 2014; 5:2679–2685.
82. Kelkar SS, Reineke TM. Theranostics: combining imaging and therapy. Bioconjugate Chem. 2011; 22:1879–1903.
83. Nie L, Chen X. Structural and functional photoacoustic molecular tomography aided by emerging contrast agents. Chem. Soc. Rev. 2014; 43:7132–7170. [PubMed: 24967718]
84. Heijblom M, et al. Appearance of breast cysts in planar geometry photoacoustic mammography using 1064-nm excitation. J. Biomed. Opt. 2013; 18:126009. [PubMed: 24343440]
85. Danielli A, et al. Label-free photoacoustic nanoscopy. J. Biomed. Opt. 2014; 19:086006. [PubMed: 25104412]
86. Wang X, et al. Noninvasive laser-induced photoacoustic tomography for structural and functional in vivo imaging of the brain. Nat. Biotechnol. 2003; 21:803–806. [PubMed: 12808463]
87. Jeon M, et al. Multiplane spectroscopic whole-body photoacoustic imaging of small animals in vivo. Med. Biol. Eng. Comput. 2014; doi: 10.1007/s11517-014-1182-6
88. Wang L, et al. Single-cell label-free photoacoustic flowoxigraphy in vivo. Proc. Nat. Acad. Sci. U. S. A. 2013; 110:5759–5764.
89. Zhang J, et al. Characterization of lipid-rich aortic plaques by intravascular photoacoustic tomography: ex vivo and in vivo validation in a rabbit atherosclerosis model with histologic correlation. J. Am. Coll. Cardiol. 2014; 64:385–390. [PubMed: 25060374]

90. Yuan K, et al. In vivo photoacoustic imaging of model of port wine stains. J. Xray Sci. Technol. 2012; 20:249–254. [PubMed: 22635179]
91. Hu S, et al. Label-free photoacoustic ophthalmic angiography. Opt. Lett. 2010; 35:1–3. [PubMed: 20664653]
92. Jiao S, et al. Photoacoustic ophthalmoscopy for in vivo retinal imaging. Opt. Exp. 2010; 18:3967–3972.
93. He G, et al. In vivo cell characteristic extraction and identification by photoacoustic flow cytography. Biomed. Exp. 2015; 6:3748–3756.
94. Wang B, et al. In vivo intravascular ultrasound-guided photoacoustic imaging of lipid in plaques using an animal model of atherosclerosis. Ultrasound Med. Biol. 2012; 38:2098–2103. [PubMed: 23069134]
95. Sussman CB, et al. Photoacoustic tomography can detect cerebral hemodynamic alterations in a neonatal rodent model of hypoxia-ischemia. Acta. Neurobiol. Exp. (Wars). 2012; 72:253–263. [PubMed: 23093012]
96. Salehi HS, et al. Design of miniaturized illumination for transvaginal co-registered photoacoustic and ultrasound imaging. Biomed. Exp. 2014; 5:3074–3079.
97. Izumi T, et al. Ultrasonic and photoacoustic imaging of knee joints in normal and osteoarthritis rats. Conf. Proc. IEEE Eng. Med. Biol. Soc. 2013; 2013:1116–1119. [PubMed: 24109888]

Imaging technology

Can advanced optical technology and sensitive ultrasound detection be developed in photoacoustic imaging for scalable visualization from single cell to whole body to capture subtle changes of disease microenvironments and realize early-stage diagnosis?

Theranostic optical probes

Can we synthesize biocompatible theranostic probes and obtain administrative approval, providing multifunctional pathophysiological information in real time, enabling precise diagnosis and personalized therapy for human disease?

Photoacoustic imaging in clinics

Can photoacoustic imaging systems be an effective preoperative and intraoperative imaging method in various clinical areas?

- Improved interrogation of complex biological systems is possible through photoacoustic imaging.
- The data generated from photoacoustic imaging has provided insights to design high sensitive and specific imaging agents and biomarkers.
- One important innovation in photoacoustic imaging has been to bridge relevant fields for early-stage theranostics.
- Technical challenges and difficulties still remain, but the clinical outlook is promising.

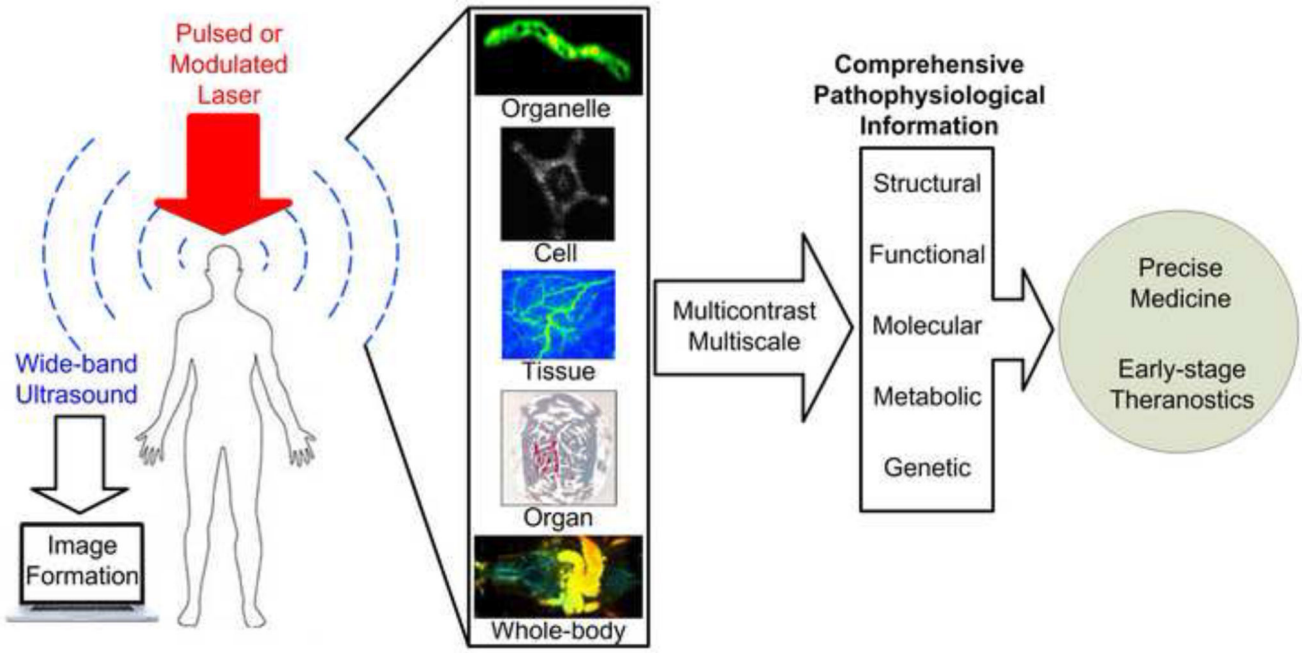

Figure 1.

Photoacoustic molecular imaging for multi-scalable biomedical applications and potential trends towards early-stage theranostics [48, 59, 85–87].

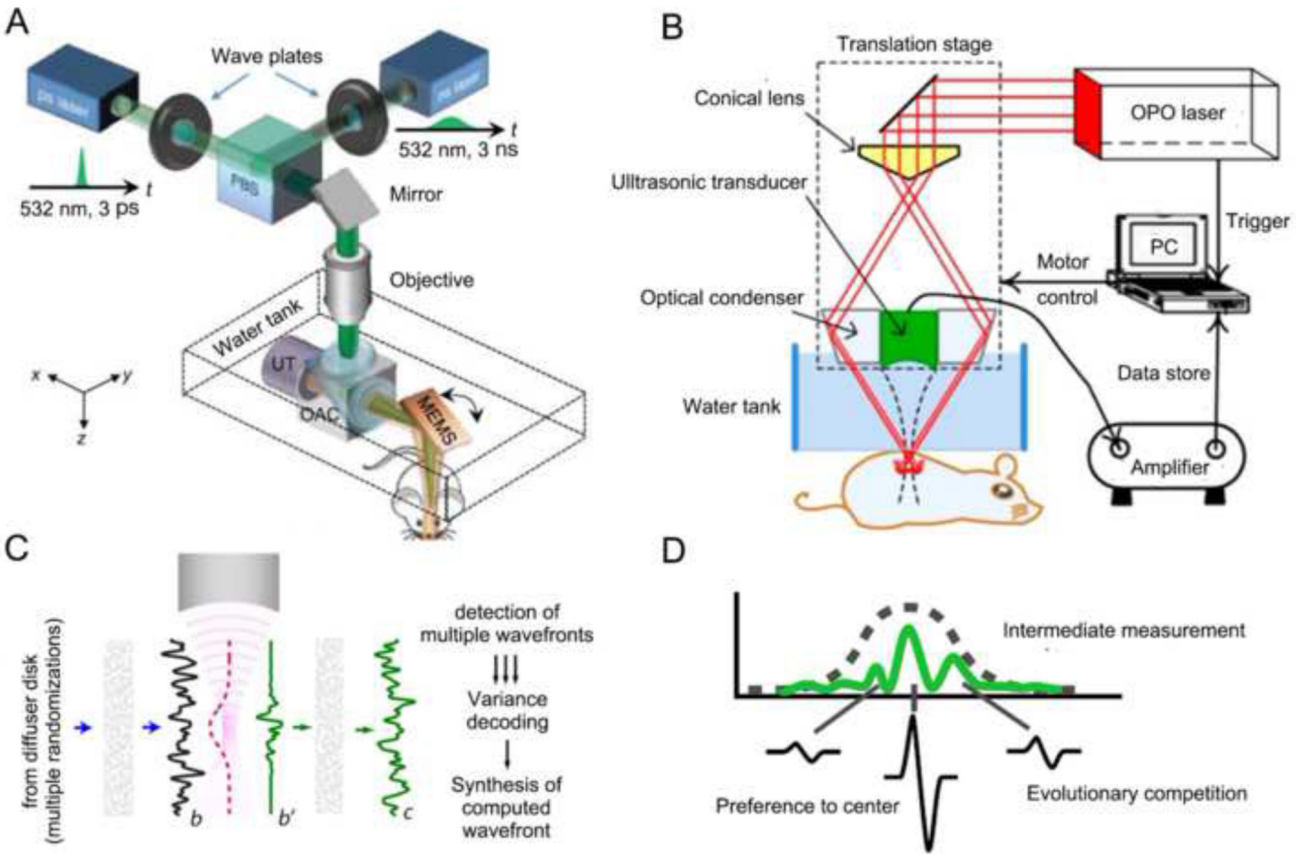

Figure 2. PAM embodiments and wavefront engineering

(A) Schematic of OR-PAM, where fast scanning is achieved by a MEMS mirror [7]. (B) Schematic of AR-PAM [6]. (C) Concept of TROVE focusing. In TROVE imaging, multiple randomized input wavefronts are frequency-shifted, decoded and time reversed [15]. (D) Gaussian-shape based PA signals to guide wavefront optimization [18]. Abbreviations: PAM (photoacoustic microscopy); OR-PAM (optical-resolution photoacoustic microscopy); OAC (optical-acoustic combiner); PBS (polarizing beam splitter); UT (ultrasonic transducer); MEMS (microelectromechanical scanner); AR-PAM (acoustic-resolution photoacoustic microscopy); TROVE (time reversal of variance encoded light).

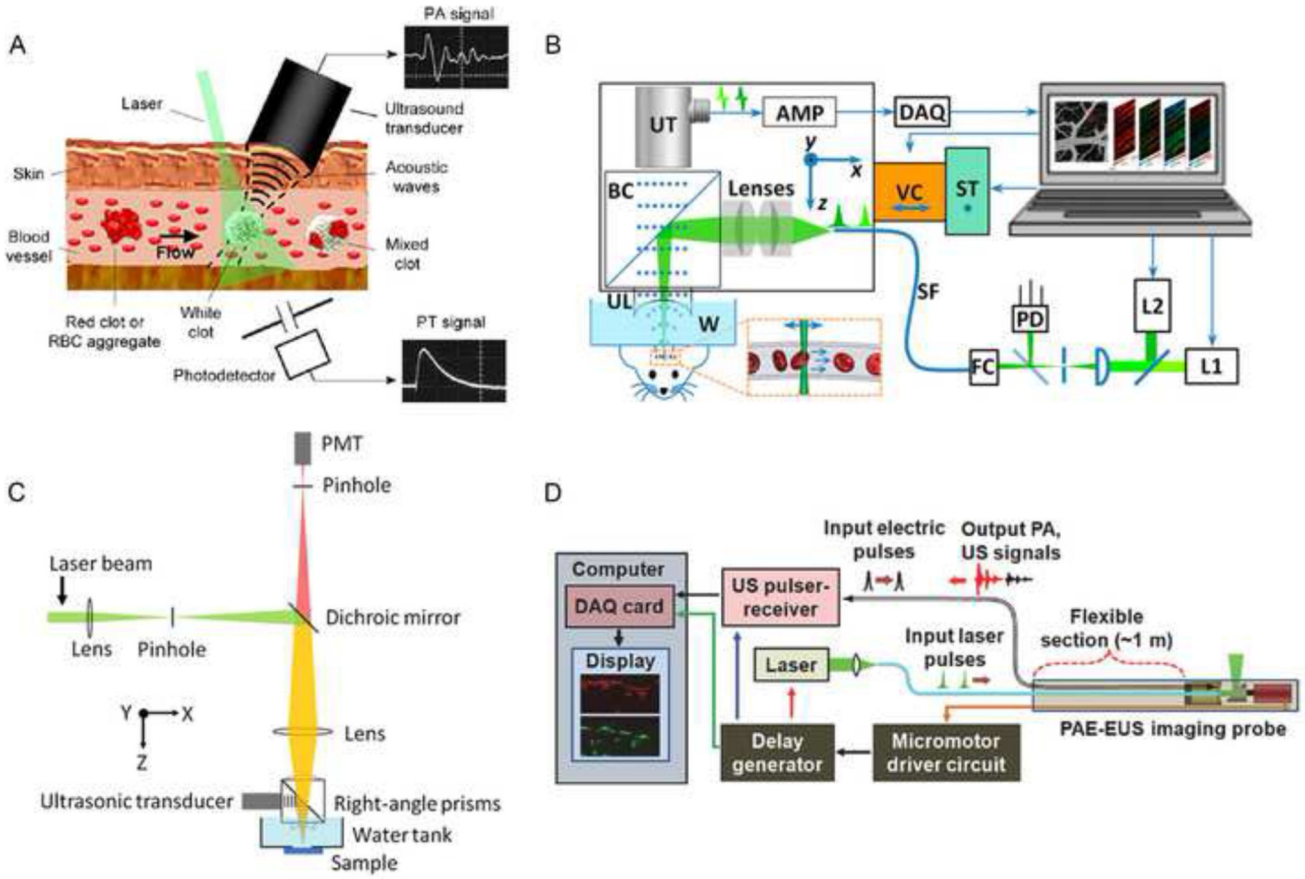

Figure 3. Multifunctional PAM platforms

(A) PAFC of RBCs in different vessels [20]. (B) PA flowoxigraphy of oxygen metabolism [88]. (C) Scheme of FRET PAM [29]. (D) Optical-resolution PAE [35]. Abbreviations: PAFC (photoacoustic flow cytometry); RBCs (red blood cells); FRET (Förster resonance energy transfer); PAE (photoacoustic endoscopy).

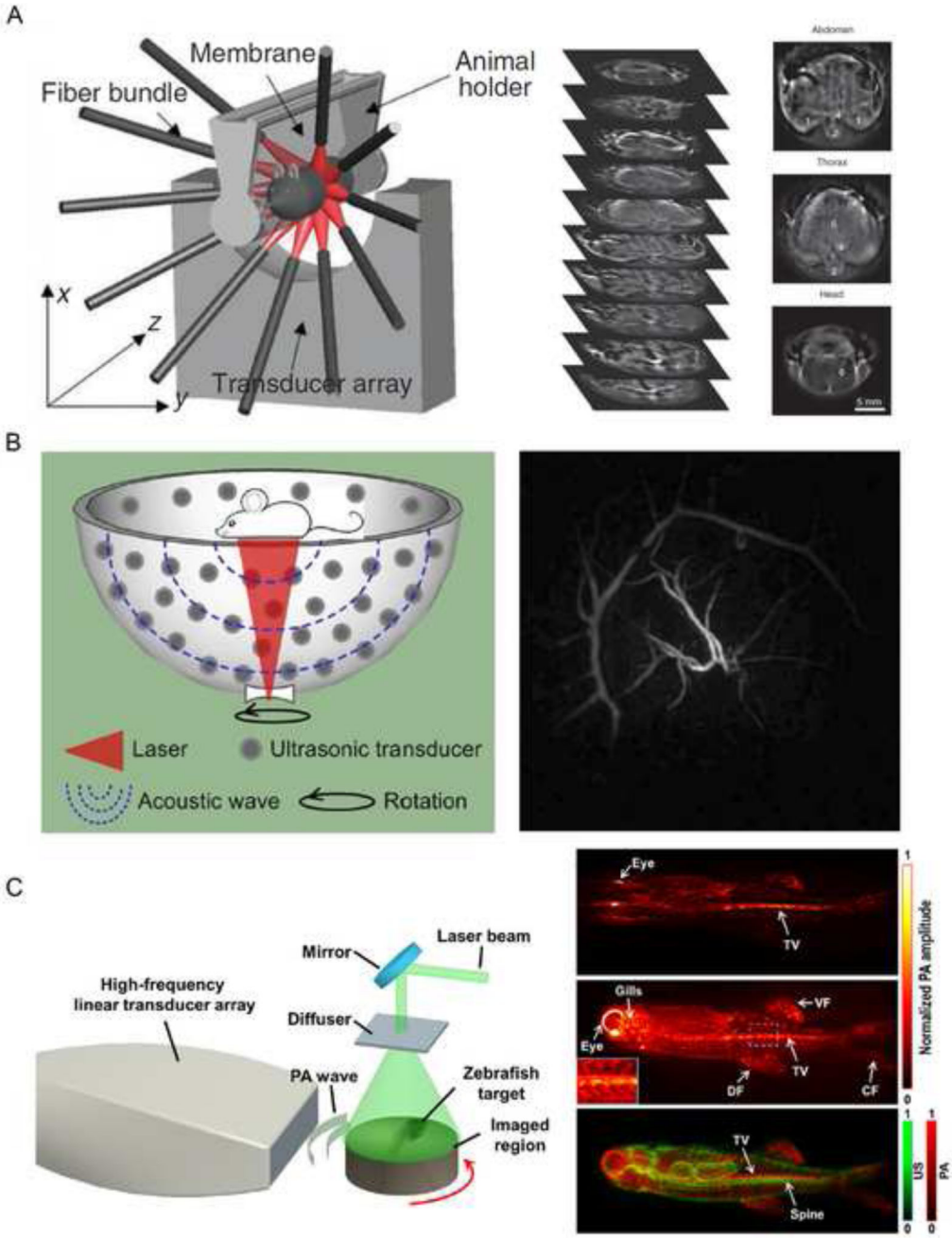

Figure 4. Major implementations of PACT

(A) *In vivo* MSOT (multispectral optoacoustic tomography) imaging of athymic mouse acquired at 750 nm [39]. (B) Anterior–posterior MIP image of the human breast by hemispherical array-based PACT [48, 50]. (C) Co-registered US/PA image of a zebrafish acquired by a high-frequency linear-array PACT system [54].

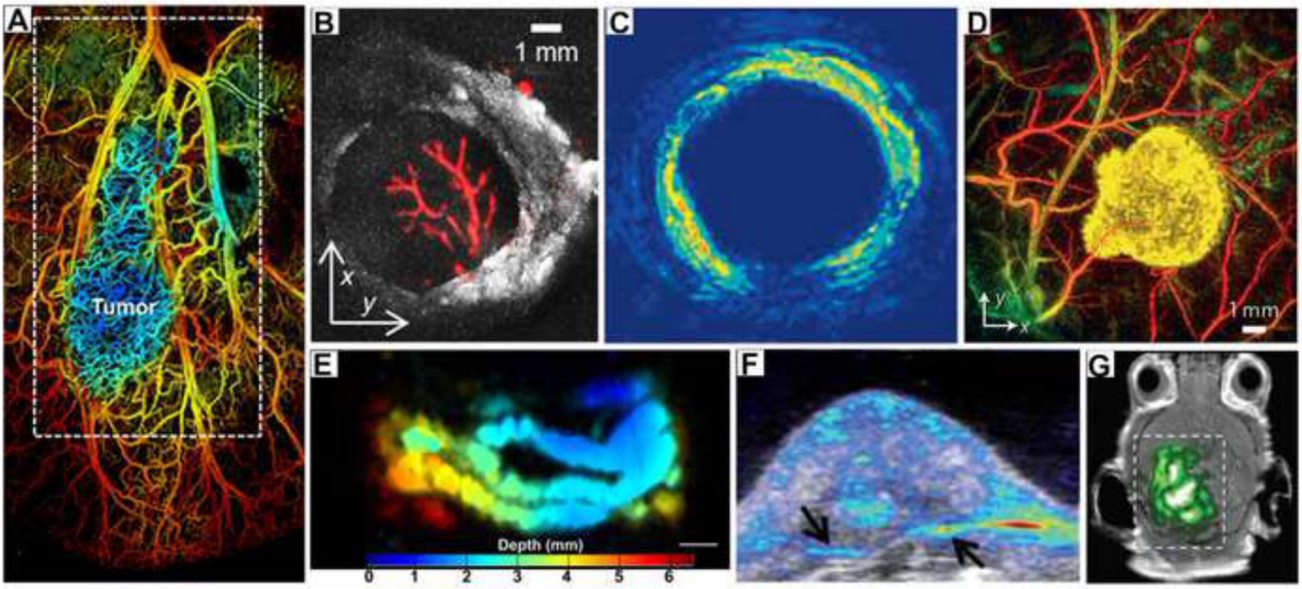

Figure 5. PAI of multiple endogenous and exogenous contrasts

(A) Microvasculature within a tumor region. The blue region indicates decreased sO_2 of the early-stage tumor [25]. (B) 3D PA images of lymph nodes at 530 nm and 1210 nm showing hemoglobin and lipid contrast, respectively [58]. (C) Intravascular PAT of lipid-rich plaques [89]. (D) *In vivo* PA image of tyrosinase labelled xenografts against the surrounding vasculature [66]. (E) PA maximum intensity projection of an intestine labeled with ZnBNc nanonaps [67]. (F) Overlaid PA and ultrasound imaging of palladium nanosheet-targeted tumor [77]. (G) PAT of a mouse brain tumor after injection with tri-modality MRI-PA-Raman (MPR) nanoparticles [63].

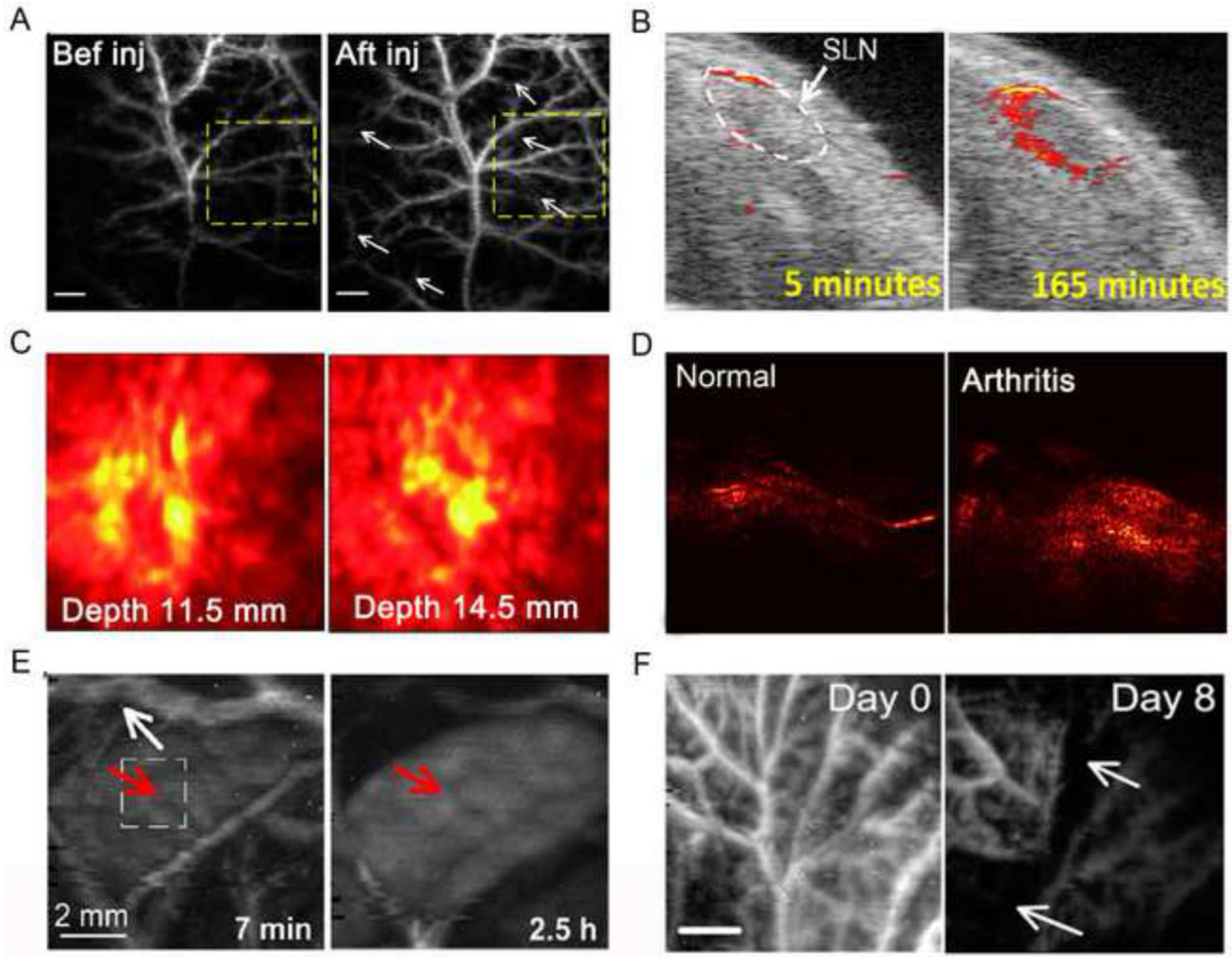

Figure 6. PAT for early-stage diagnostic, drug metabolism, and therapy monitoring

(A) Nutrition supply vasculature on a tumor was imaged by PAM six hours after GO injection [6]. (B) 3D US/PA images of SLNs show the increased PA signal following the injection of Si-AuNPs [79]. (C) PA mamoscope images of tumor vasculature in a patient with invasive ductal carcinoma [78]. (D) PAT images of a rat ankle joint, showing increased PA signal associated with inflammatory arthritis [80]. (E) *In vivo* PA images of spleen in a rat after injection of GNS, illustrating that the signals significantly increased in spleen compared with decreased PA signal in vascular [81]. (F) Scalable PAM images of tumor vasculature using GO-Cy5.5-Dox contrast, depicting that the angiogenic vessels were greatly disrupted 8 days after chemotherapy [6]

Table 1

Summary of the major advances, trends, and challenges of PAI systems for clinical translation

PA imaging system	Features	Technique advances and trends	Disease models	Translational challenges	References
PAM	Laser focusing, high ultrasound frequency, raster scanning	High frame rate, wavefront engineering, microelectromechanical systems	Melanoma imaging, port-wine stains, ophthalmology diagnosis	Shallow penetration depth, limited FOV	[59, 90–92]
PAFC	Single cell detection, high resolution	Specific disease targets, ultrasensitive abnormal cells detection	Circulating tumor cells, hematologic diseases	Shallow detection depth, low sensitivity	[24, 93]
PAE	Circumferential sector scan, interior imaging	Miniaturized probe, coregistered PAE/EUS system	Gastrointestinal tract imaging, atherosclerosis detection, lymph node imaging	Probe size, motion artifacts, robustness	[35, 36, 94]
PACT	Circular scanning, inverse reconstruction algorithm, large FOV	Detection geometries, parallel data-acquisition, sophisticated reconstruction	Human breast cancer, primate brain imaging through skull, hypoxic-ischemic encephalopathy	Strong artifacts, suboptimal spatial resolution and imaging speed	[10, 50, 95]
PA mammoscope	Flat ultrasonic transducer array, fast DAQ, large field-of-view (FOV).	NIR laser or microwave excitation, real-time imaging	Human breast cancer diagnosis	Patient-instrument interface, and relatively low spatial resolution	[84]
Ultrasound array based PAT	Dual-modality, adaptable from clinical ultrasound system	Handheld probe, portable	SLN mapping, human ovarian tissue, rat bone and joint imaging	Low SNR, Imaging accuracy	[64, 96, 97]

Trends Biotechnol. Author manuscript; available in PMC 2017 September 15.